Probing Interfacial Organization in Surface Monolayers Using Tethered Pyrene. 1. Structural Mediation of Electron and Proton Access to Adsorbates

ARTICLE *in* THE JOURNAL OF PHYSICAL CHEMISTRY B · SEPTEMBER 2005

Impact Factor: 3.3 · DOI: 10.1021/jp0513824 · Source: PubMed

4 AUTHORS, INCLUDING:

Gary J Blanchard
Michigan State University
186 PUBLICATIONS **3,953** CITATIONS

SEE PROFILE

Probing Interfacial Organization in Surface Monolayers Using Tethered Pyrene. 1. Structural Mediation of Electron and Proton Access to Adsorbates

Monika Domińska,[†] Krystyna Jackowska,[†] Paweł Krysiński,*[,†] and G. J. Blanchard*[,‡]

Department of Chemistry, University of Warsaw, 02-093 Warsaw, Pasteura 1, Poland, and Department of Chemistry, Michigan State University, East Lansing, Michigan 48824-1322

Received: March 16, 2005; In Final Form: June 23, 2005

We have synthesized and characterized a family of self-assembled monolayers containing pyrene derivatives on gold and indium-doped tin oxide (ITO) substrates. The covalently bound pyrene functionalities serve as either spectroscopic or electrochemical probes of their immediate environment, and we explore their electrochemical response in this paper. When these compounds are the only constituents bound to the interfaces, the molecules enjoy significant structural freedom. The addition of aliphatic adsorbates to the interfaces serves to place the pyrene derivatives in a more restricted environment. Cyclic voltammetry shows that the organization of a monolayer with pyrene derivatives, and the position of the terminal pyrene within such monolayer, depend sensitively on the length of the pyrene tether and the presence or absence of aliphatic interfacial species, as well as the identity of the substrate.

Introduction

The development of self-assembling monolayer chemistry, pioneered by Nuzzo and Allara for disulfides and thiols on gold[1] and subsequently expanded to a range of different surfaces and bonding chemistries, has served as a versatile and powerful means for controlling interfacial properties. Self-assembled monolayers (SAMs) provide ready access to experimental systems where the physical properties of interfaces can be modified and the chemical identities of the interfacial species can be examined by spectroscopic and electrochemical techniques. Because of the structural versatility of SAMs and the relative ease with which they can be synthesized, there is a great deal of practical interest in these materials as potential chemical and biological sensing systems.

Since the original work on thiol/gold chemistry and carboxylic acid/alumina bonding strategies,[2,3] there has been a significant effort aimed at making SAM structures more robust. The gold−sulfur bond responsible for alkanethiol/gold monolayer formation is modest in strength, and this fact is ultimately responsible for the labile nature of this family of interfaces.[4,5] Indeed, there is interest not only in the formation of enthalpically more robust mono- and multilayers but there has also been a sustained effort to create interfacial layers on oxide surfaces for a variety of fundamental and practical reasons. The growth of interfacial mono- and multilayer structures using metal bisphosphonate and related ionic interlayer linking chemistry was developed by the Mallouk, Thompson, and Katz groups[6−11] and is in wide use today. Similarly, there have been several reports of covalent interlayer linking chemistry to form robust, simple mono- and multilayer interfaces on oxide surfaces such as indium-doped tin oxide (ITO) and SiO_x.[12,13] Until recently, the chemical methodologies appropriate for layer formation on relatively well organized metal surfaces has not been accessible to the chemical approaches used on oxide surfaces. Recent work by Krysinski and Blanchard has shown that the electrochemical formation of an oxide layer on a gold surface can be reacted with acid chlorides, which serve to stabilize the gold oxide layer by forming a gold ester.[14] This advance has brought the chemistry previously restricted to layer growth on oxide surfaces to more organized metallic substrates.

Given the broad range of means available for the creation of interfacial structures, it is important to consider the ways in which these interfaces can be characterized. The "standard" techniques such as optical ellipsometry, contact angle measurement, and infrared (IR) spectroscopy are not well suited to providing direct information on the molecular scale organization of these interfacial structures. This spatially averaged information is very useful, but recently it has been shown that such data can be misleading.[15] If these interfacial structures are to be used for chemical sensing, the intrinsic selectivity of the interface, which is determined at the molecular level, must be probed directly. It is this purpose which we address here. We have designed a series of SAMs that contain pyrene derivatives bound covalently to either gold or oxide (ITO, SiO_x) surfaces. Pyrene is a well-known chromophore used to characterize local "polarity", and both its time- and frequency-domain spectral properties can be used to measure short-range organization within mono- and multilayer structures. The electrochemistry of pyrene is also well understood, particularly with respect to its oxidative instability. Interrogating both the spectroscopic and electrochemical behavior of covalently bound pyrene on metallic and oxide substrates allows us to gain access to local organization in these systems as a function of the interface chemical identity. In this first of two papers, we report on the electrochemical response of tethered pyrene derivatives on Au and ITO substrates. We have found that the organization of several of these monolayers depends sensitively on both interface composition and on the existence and polarity of any liquid overlayers on the interface.

* To whom correspondence should be addressed.
[†] University of Warsaw.
[‡] Michigan State University.

10.1021/jp0513824 CCC: $30.25
Published on Web 07/29/2005

Experimental Section

Chemicals. 1-Pyrenebutyric acid (97%), 1-pyrenemethylamine hydrochloride (95%), octadecylamine (97%), 2-mercaptoethylamine (95%), 11-mercaptoundecanoic acid (95%), 10-hydroxydecanoic acid, octadecylmercaptan (98%), 1-hexadecylamine (98%), *N*,*N*′-dicyclohexylcarbodiimide (DCC) (99%), adipoyl chloride (≥99%), 4-methylmorpholine (≥99.5%), triethylamine (≥99%), perchloric acid (70%), ruthenium (III) hexamine chloride (98%), potassium ferrocyanide (99%), lithium perchlorate (99.99%), cyclohexane (99%), 1-pentanol (≥99%), and acetonitrile (anhydrous) were obtained from Aldrich. Dichloromethane and chloroform were obtained from POCH or from Mallinckrodt Chemicals. Aqueous solutions were prepared from Milli-Q water.

Preparation of Pyrene on Short Tether for Gold Substrate. Pyrene bound to gold using a "short tether" (the cysteamide of pyrenebutyric acid, designated P7, where the number 7 indicates the number of atoms between the attaching headgroup and the pyrene moiety) was synthesized according to a standard procedure for peptide synthesis in solution.[16] Pyrenebutyric acid and cysteamine were dissolved in dichloromethane and then cooled to 0 °C. After 1 h of stirring, DCC in dichloromethane was added and the reaction proceeded at room temperature for 12 h. The final product was purified by silica gel column chromatography (Silica gel 60 from Merck, particle size 0.040−0.063 mm) and analyzed by IR spectroscopy.

Gold Substrate Preparation. Gold ball electrodes were cleaned in piranha solution (3:1 concentrated H_2SO_4: 30% H_2O_2). Caution! Piranha solution reacts violently with organic matter and should be handled with extreme care! The cleaned electrodes were rinsed with water and polarized cyclically (scan rate 100 mV/s) in the −250 to +1650 mV potential range in 1 M $HClO_4$ until reproducible voltammograms were obtained. Next, electrodes were removed from the cell, washed with distilled water, and dried with a stream of nitrogen. The area of the gold ball electrode was 0.135 cm^2, which was determined from the cyclic voltammetry (CV) of a $K_4[Fe(CN)_6]$ solution.[17]

Silica Substrate Preparation. Silica slides were cleaned by immersion in piranha solution for ca. 20 min and then rinsed with water and dried in a stream of nitrogen.

ITO Substrate Preparation. ITO films deposited on silica substrates were cleaned by rinsing with water, ethanol, and acetone, consecutively.

Monolayer Preparation. To create a monolayer of P7 on gold, the substrate was exposed to solution of P7 in dichloromethane for 12 h. The SAM-covered gold electrode was then rinsed with dichloromethane and dried in a stream of nitrogen, then washed with distilled water and dried in a stream of nitrogen. The monolayer of the nominally buried P7 was obtained by immersing a gold electrode into a solution of P7 and octadecyl mercaptan (ODM) (1:1) in dichloromethane for 12 h. For deposition of a monolayer of pyrene tethered a longer distance from the gold substrate, the substrate was first exposed to a solution of 11-mercaptoundecanoic acid (MUA) in dichloromethane for 12 h. The resulting SAM-covered gold substrate was rinsed with dichloromethane, dried in a stream of nitrogen, and immersed in a solution of pyrenemethylamine and DCC (1:1) in dichloromethane for 12 h to form a monolayer of mercaptoundecanoic acid pyrenemethylamide (P13). To synthesize a monolayer of "buried" P13, a substrate covered with a monolayer of MUA was immersed in a dichloromethane solution containing pyrenemethylamine, hexadecylamine, and DCC (1:1:2) for 12 h.

Monolayers on ITO substrates were synthesized by reaction of the substrate with adipoyl chloride (0.3 mL) in dry acetonitrile (10 mL), using 4-methylmorpholine (0.3 mL) as a Lewis base, under reduced pressure for 1 h. The reacted substrates were removed from solution, rinsed with dry acetonitrile and ethyl acetate, and dried under a stream of dry nitrogen. We synthesized monolayers of tethered pyrene either as the only constituent or as a co-constituent with a long-chain aliphatic moiety. These monolayers were obtained by exposing the adipoyl chloride covered substrate either to a 2 mM solution of pyrenemethylamine in dichloromethane, producing a single-component monolayer of the pyrenemethylamide of adipic acid, P8. For the corresponding monolayer where P8 is "buried", a dichloromethane solution of pyrenemethylamine and hexadecylamine (1:1) is reacted under reduced pressure for 0.5 h. Following this reaction, the substrate was removed from solution, rinsed with dichloromethane and ethyl acetate, and dried under a stream of dry nitrogen. For pyrene tethered further from the substrate, the adipoyl chloride covered substrate was first reacted with a 2 mM solution of 10-hydroxydecanoic acid in dichloromethane. Following the addition of this C_{10} chain, the substrate was removed from the reaction vessel, rinsed with dichloromethane and ethyl acetate, and dried under a stream of dry nitrogen. The substrate thus covered with adipic acid mono-(10-carboxy)-decyl ester was then exposed either to pyrenemethylamine and DCC (1:1) (to form pyrenemethylamide-10-decyl ester, P19) in dichloromethane or to pyrenemethylamine, hexadecylamine, and DCC (1:1:1) in dichloromethane under reduced pressure for 0.5 h. The reacted substrate was removed from solution, rinsed with dichloromethane and ethyl acetate, and dried under a stream of dry nitrogen.

Electrochemistry. Electrochemical measurements were made with a computer-controlled electrochemical workstation (CH instruments Model 604B and Model 650), using a three-electrode cell with a Pt wire counter electrode. All potentials are quoted vs a $Ag/AgCl/3\ M\ KCl_{aq}$ reference electrode. Experiments were carried out in aqueous 0.01, 0.05, 0.1, 0.5, and 1 M $HClO_4$ (keeping the ionic strength of 1 M constant by the addition of the appropriate amount of $LiClO_4$), in aqueous 1 mM $K_4[Fe(CN)_6]$ in 0.5 M $LiClO_4$, and in aqueous 1 mM $[Ru(NH_3)_6]Cl_3$ in 0.1 M $LiClO_4$.

Langmuir Trough Experiments. Langmuir measurements were made with a commercial trough (Nima Technology). Pyrenebutyric acid and octadecylamine solutions (2 mg/mL) were used as surfactants. Several solutions with varying pyrenebutyric acid to octadecylamine molar ratios were spread on the water surface.

Results and Discussion

Pyrene Derivatives Exposed to Electrolyte Solution. The purpose of this work is to demonstrate and characterize a group of SAMs modified with pyrene derivatives, with an eye toward the application of these monolayer species as spectroscopic and electrochemical probes of their immediate environment. We have investigated pyrene derivatives bound covalently to gold and ITO substrates by CV. We show in Figure 1 the cyclic voltammograms of our pyrene derivatives bound covalently to gold and ITO. In the first scan for each voltammogram we observe an irreversible peak with a maximum above 900 mV. A pair of new, broad redox peaks appears in subsequent scans between 200 and 300 mV. We assign these features to two pairs of poorly resolved redox peaks, centered near 210 and 320 mV. Previous work has shown that these peaks are associated with the several possible diol/dione species that are the stable oxidation products of the pyrene ring system.[18]

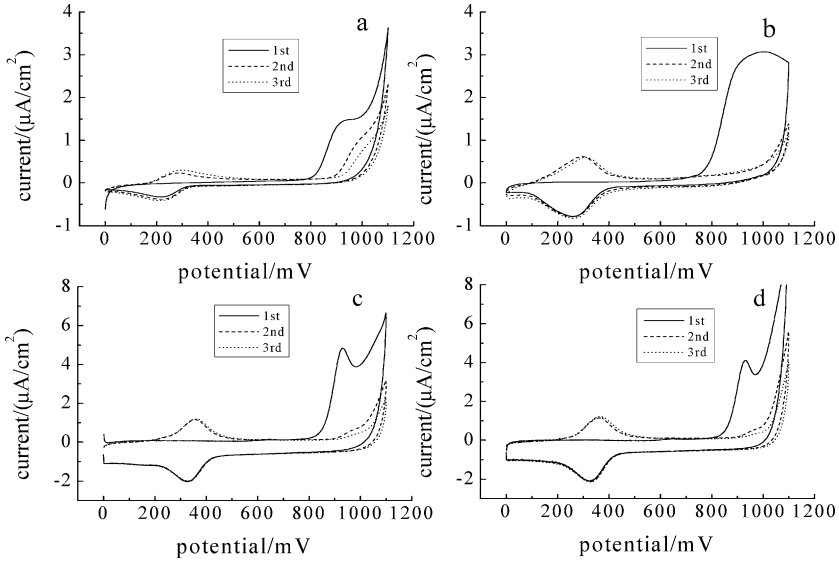

Figure 1. Cyclic voltammograms of: (a) P7 on gold in 0.1 M $HClO_4$, sweep rate 2mV/s; (b) P13 on gold in 0.1 M $HClO_4$, sweep rate 5 mV/s; (c) P8 on ITO in 1 M $HClO_4$, sweep rate 20 mV/s; (d) P19 on ITO in 1 M $HClO_4$, sweep rate 20 mV/s.

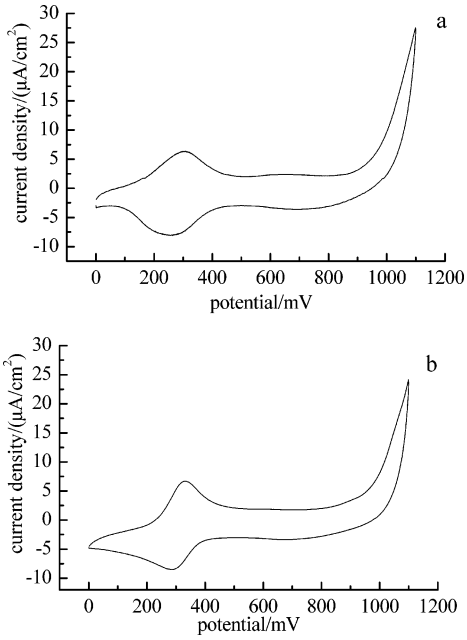

Figure 2. Cyclic voltammograms of (a) P7 and (b) P13 on gold in 1 M $HClO_4$. The sweep rate is 20 mV/s. Charge under the anodic peak is 2.105 μC for (a) and 3.106 μC for (b).

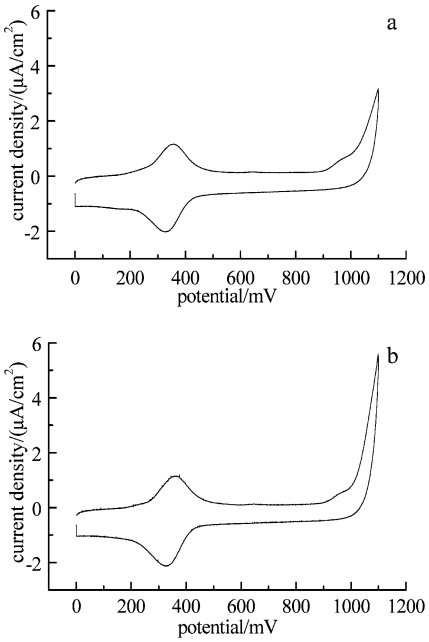

Figure 3. Cyclic voltammograms of (a) P8 and (b) P19 on ITO in 1M $HClO_4$. The sweep rate is 20 mV/s. Charge under the anodic peak is 1.048 μC for (a) and 1.345 μC for (b).

On the basis of the analysis of electrochemical reactions of surface-bound pyrene on gold and ITO surfaces reported in the literature,[19] the voltammograms presented in Figures 2 and 3 can be assigned to 1,6-pyrenedione/1,6-dihydroxypyrene (a pair of CV peaks centered around 0.32 V) and 1,8-pyrenedione/1,8-dihydroxypyrene, which is shifted to more negative values by ca. 100 mV.[18]

The electrode coverage with various pyrene derivatives was evaluated with use of CV. The amount of pyrene derivatives on the electrode surface was calculated from the charge under the anodic peak from the voltammograms recorded in aqueous 1 M $HClO_4$ electrolyte solution (Figures 2 and 3) at a low sweep rate (as specified in figure captions). Integration of this peak yielded a surface coverage (assuming a 2 electron/2 proton process[18]) of ca. 4.4×10^{-11} mol/cm^2 for P7 and 1.7×10^{-11} mol/cm^2 for P13. These same measurements on an ITO substrate yield a surface coverage of 1.2×10^{-11} mol/cm^2 for P8 and 8.4×10^{-12} mol/cm^2 for P19. To assess the maximum theoretical coverage for our pyrene derivatives on a given substrate, one has to evaluate the minimum area that can be occupied by a single pyrene ring system with its hydrocarbon tail outstretched from the surface in an all-trans configuration. For this purpose we have used the Langmuir technique. Unfortunately, because of the finite solubility of pyrenebutyric acid in water, we could not produce a pressure/area isotherm over the required phase transition range for this compound. Therefore, we have investigated the mixed pyrenebutyric acid/octadecylamine system with various pyrenebutyric acid mole fractions on a water subphase (Figure 4a). It was possible to obtain the pressure−area isotherms of this binary system for up to a 1:1 ratio of the two constituents. By assumption of additive behavior for such a binary mixture on the interface, a plot of the area per molecule as a function of the mole fraction of pyrenebutyric acid in octadecylamine allows us to estimate

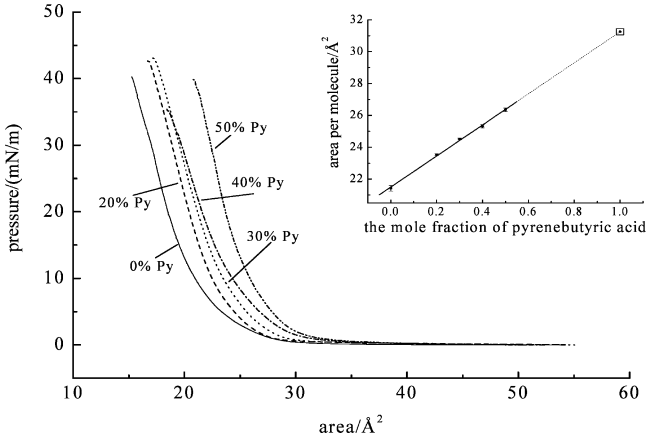

Figure 4. Pressure−area isotherms for pyrenebutyric acid and octadecylamine system. Inset: Area per molecule as a function of mole fraction of pyrenebutyric acid in mixture of octadecylamine with different concentrations of pyrenebutyric acid. The error bar on the data point is representative of the uncertainty in these measurements.

the area occupied by a single pyrenebutyric acid molecule to be 31.2 Å^2 (Figure 4b). This value is comparable to that of sterols in a monolayer: 37 Å^2/molecule for cholesterol.[20] The value of 31.2 Å^2/molecule is entirely reasonable on geometric grounds. For a rigid molecule, one can estimate an area of ca. 26 Å^2/molecule based on a molecular mechanics calculation, not taking into account any motional freedom or alternative conformers of the pyrenebutyric acid molecule. Taking the value of 31.2 Å^2/molecule for our pyrene derivatives, we estimate the maximum surface coverage of pyrene on the electrode surface to be 5.3×10^{-10} mol/cm^2, indicating that the surface coverage we obtain is well below that of a full monolayer.

We used cyclic voltammetry to assess the organization of pyrene-containing monolayers on Au and ITO substrates. Typically, well organized, hydrophobic layers block electron transfer from hydrophilic redox probes present in the supporting electrolyte solution to the conductive substrate. For these interfaces, we have used hexammineruthenium (III) (1 mM) as the redox-active probe, which produces a quasireversible CV curve (not shown). Our data point to poorly organized monolayers, consistent with previous literature reports showing that when cysteamine molecules are used as anchoring moieties to gold (P7), the resulting monolayer adopts a predominantly gauche conformation.[21,22,23] For such a conformation, one would expect a monolayer with numerous access points to the substrate. For P13, where mercaptoundecanoic acid is the anchoring species, the amide group, formed by reaction of MUA with pyrene−methylamine to form P13, should be solvated, also resulting in a poorly organized monolayer. Thus, the hydrophilic hexammineruthenium(III) redox probe, regardless of the length of a tether anchoring the pyrene ring system to the substrate, can gain access to the electrode surface, resulting in quasireversible voltammetric behavior.

By consideration of the sub-monolayer coverage and relative ease of diffusion for the hexammineruthenium (III) cation through these layers, as well as the fact that protons participate in the redox reactions (Scheme 1), we should observe a pH dependence in the plots of the potential of the midpoint, E_m. Between the maximum of the oxidation peak E_{pa} and the potential of the maximum of the reduction peak, E_{pc}, a gradual decrease in pH should lead to a positive shift of the midpoint potential by about 60 mV per unit pH if the ratio of protons to electrons is close to one ($2H^+$, $2e^-$) in the reaction scheme (Scheme 1) that leads to either 1,6-pyrenedione/1,6-dihydroxypyrene or 1,8-pyrenedione/1,8-dihydroxypyrene.

Figure 5 shows the shifts in peak potentials to more positive values with decreasing solution pH. On the basis of CVs for pyrene derivatives obtained in different perchloric acid concentrations we can determine the dependence of the midpoint potential between the anodic and cathodic peaks, E_m, as a function of pH (Figure 6). The experimental data show that the slope of plots of the midpoint potential, E_m, is ca. −45 mV/pH unit for both adlayers on gold, and for the ITO substrate, the slope of E_m vs pH is ca. −53 mV/pH unit. There are several interesting features contained in these data. The first is that the pyrene derivatives anchored to either Au or ITO appear not to undergo a full $2H^+/2e^-$ redox reaction. Rather, the calculated ratio of protons to electrons involved in the unit redox reaction is close to 0.8. Even though this finding is similar to data reported for the ubiquinone/ubiquinol (UQ/UQH_2) redox couple confined to the mercury surface by a phospholipid monolayer,[24,25,26] where deviations from the expected 60 mV/(unit

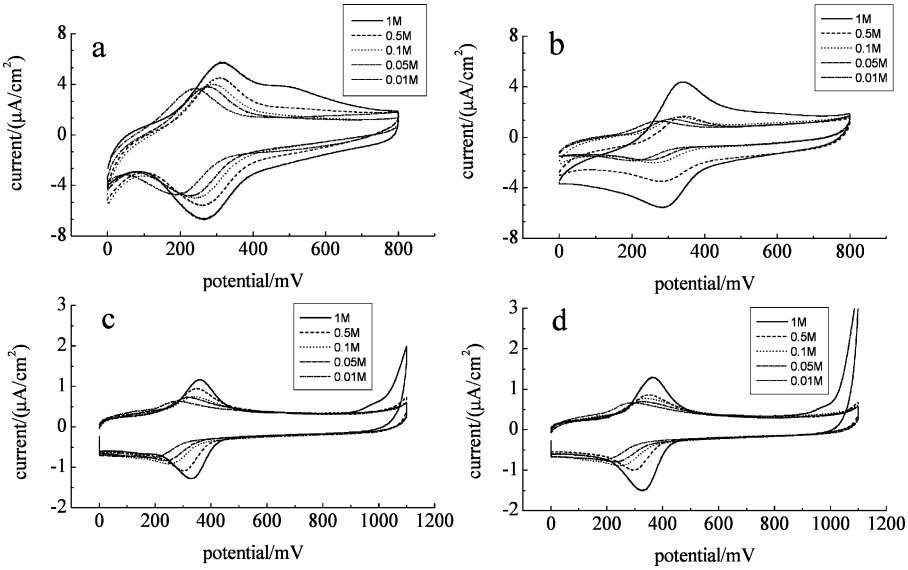

Figure 5. Cyclic voltammograms for the pyrene-containing adlayers: (a) P7 on gold; (b) P13 on gold; (c) P8 on ITO; (d) P19 on ITO, all in 1, 0.5, 0.1, 0.05, and 0.01 M aqueous $HClO_4$. The ionic strength is maintained at 1 M for all solutions by aqueous $LiClO_4$. The sweep rate was 20 mV/s for all CVs.

SCHEME 1: Schematic of the Redox Reactions Characteristic of the Pyrene Moiety (for Clarity, This Drawing Shows only the P7 Molecule)[a]

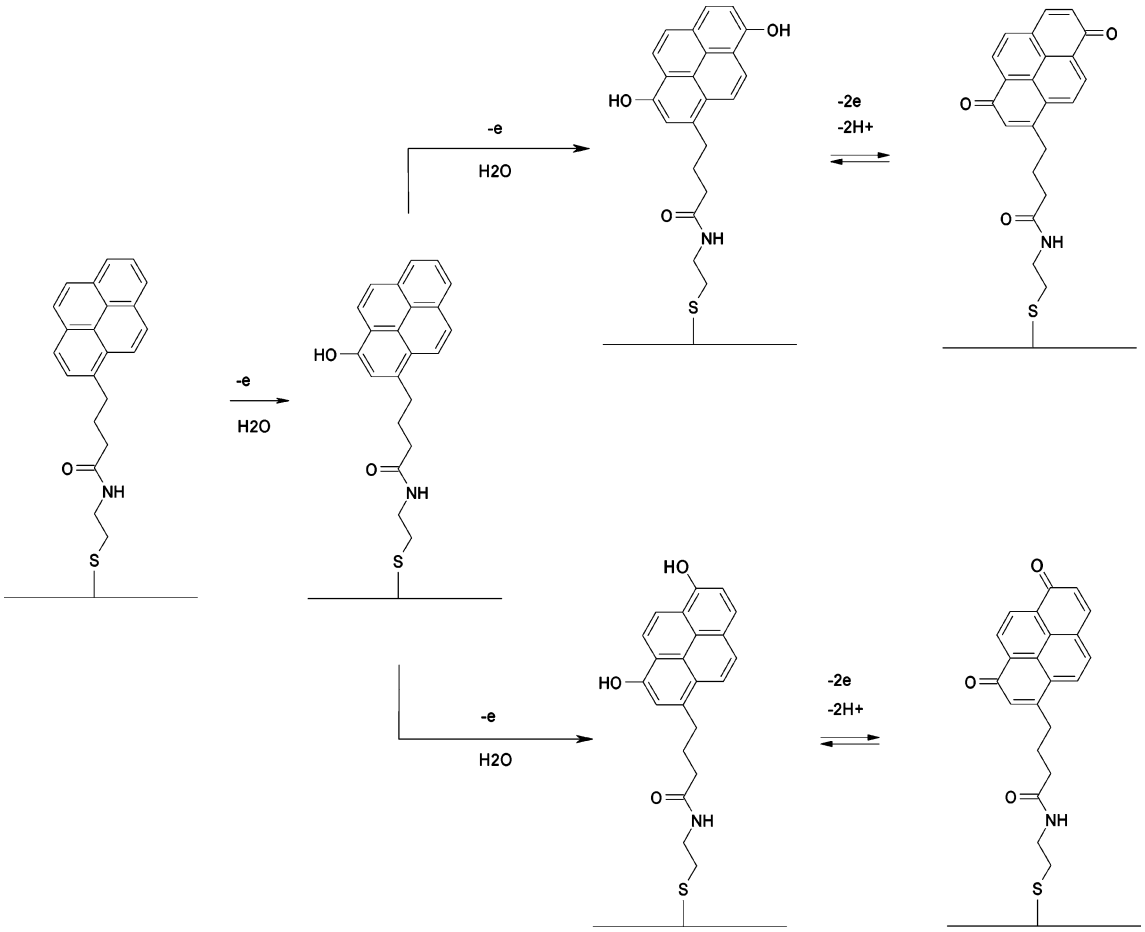

[a] The structures shown are not an exhaustive list of the reaction products but are representative of the dominant species.

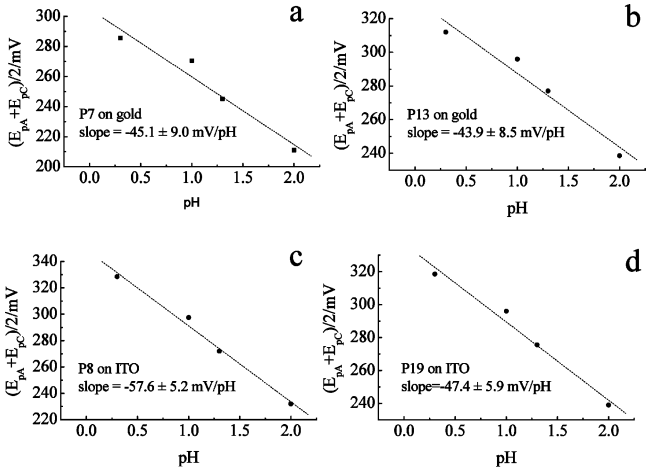

Figure 6. Dependence of the midpoint potential, E_m, on the pH of perchloric acid aqueous solutions for (a) P7 on gold, slope $= -45.1 \pm 9.0$ mV/pH, (b) P13 on gold, slope $= -43.9 \pm 8.5$ mV/pH, (c) P8 on ITO, slope $= -57.6 \pm 5.2$ mV/pH, and (d) P19 on ITO, slope $= -47.4 \pm 5.9$ mV/pH. For all scans, the sweep rate was 20 mV/s. Uncertainties indicated in all panes are $\pm 1\sigma$.

pH) were observed for UQ, we believe that the observed deviation from a 1:1 H^+:e^- ratio is mainly due to uncertainty in the experimental data (the 1 M $HClO_4$ solution, in particular, is of concern).

In the following section, we consider the rate constants for the redox processes that are responsible for the observed behavior. Our previous work has shown that pyrene redox chemistry is explained well in the context of a $2H^+/2e^-$ reaction,[18] and we evaluate the rate constants based on this knowledge. We caution, however, that there are other possible explanations for our data. It is also possible for a $1H^+/1e^-$ reaction to account for our findings, particularly for reactants in a confined space or for more complex schemes involving disproportionation and/or further reduction to be operative (Figures 6). These possibilities have been pointed out previously for the UQ/UQH_2 redox pair.[25] One should also consider that the chemical reaction, involving a protonation step during $Py(O)_2$ reduction and a deprotonation in $Py(OH)_2$ oxidation, is usually the rate-determining step, with electron transfer being in quasiequilibrium.

We have used AC voltammetry to study the redox kinetics of several pyrene derivatives bound as monolayers to Au and ITO. This technique has proven to be particularly useful for the investigation of redox reactions in layered assemblies on electrodes[27−30] because a variety of information can be obtained from such data. First, for a given reversible reaction, the peak position of the voltammogram gives information on the formal potential of the surface redox reaction. As shown in Figure 7, the peak potential values are lower by ca. 58 mV than the formal potential values obtained during the CV experiments by extrapolating the slope of the midpoint potential, E_m vs pH to pH $= 0$. Since the alternating current (AC) experiments were carried out in 0.1 M $HClO_4$ (pH $= 1$), this smaller value is due to the dependency of the overall process on proton concentration. It is also important to note that the difference in peak position

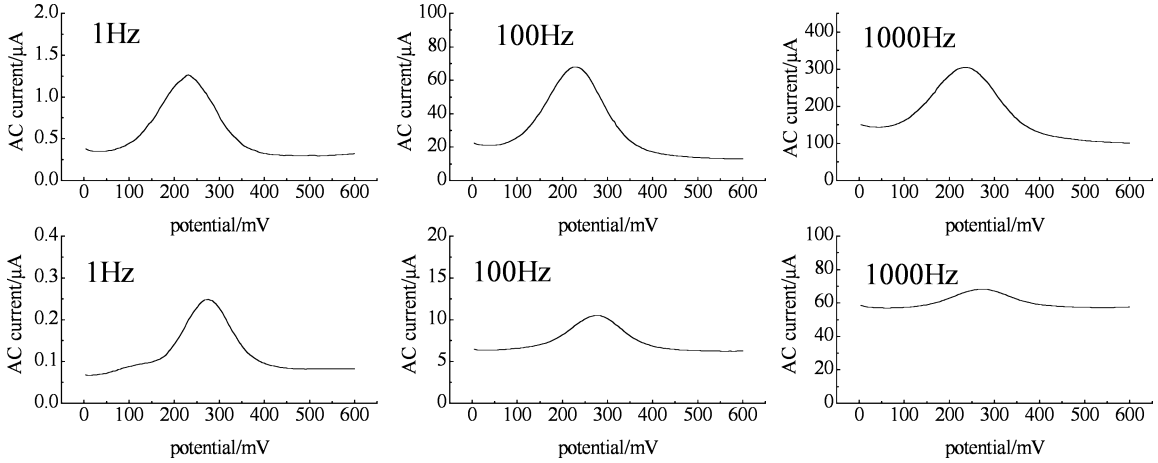

Figure 7. AC voltammograms for P7 (top row) and P13 on gold in 0.1M $HClO_4$. AC frequencies are indicated in each pane.

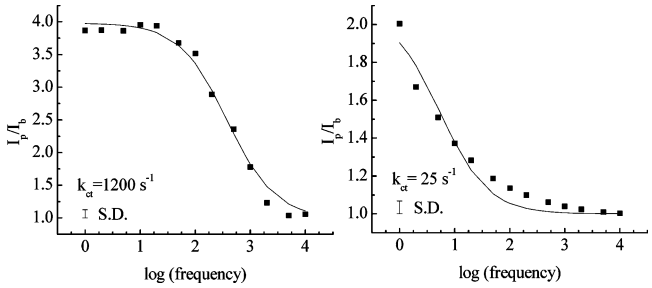

Figure 8. $I_{peak}/I_{background}$ vs log(frequency) plots of monolayers of P7 (left) and P13 (right) on gold. The solid lines represent fits to the data (black squares) using a Randles equivalent circuit.[27,28] We estimate the uncertainty in k_{ct} to be ± 10%.

between P13 and P7 is slightly higher than that obtained from direct current CV, yielding the $\Delta(\Delta G°)$ value of ca. 7 kJ/mol.

In these AC voltammograms (Figure 7), we observe a decrease in the peak-to-background current ratio with increase in frequency. Such changes in the magnitude of the ac peak current with the changing frequency of the AC voltage provide information about the rate constant of the reaction. These data are a series of AC voltammograms taken at three selected frequencies to illustrate the behavior of the pyrene redox reaction as a function of tether length and whether the tether length influences the redox kinetics. Creager's group has shown that it is possible to assess the charge-transfer rate constants from such voltammograms by using a relatively simple Randles equivalent circuit for the impedance of an electrode coated with a redox-active film.[27−29] We note that, for the systems we consider here, it can be the chemical step (e.g., protonation/deprotonation) that is rate determining, so the quantitative evaluation of the charge-transfer rate constant, k_{ct}, should be viewed with some caution.

With these caveats in mind, we have used Creager's methodology[27−29] and present the AC data from Figure 7 in the form of the peak current to background current ratio, I_p/I_b vs log(AC frequency) for a series of voltammograms recorded over a range of frequencies (Figure 8). Plotting the AC voltammetry data in the manner shown in Figure 8 reveals three distinct regions of the reaction frequency dependence. At low frequencies, the current ratio attains a plateau value that is indicative of the amount of pyrene on the electrode surface; at high frequencies this ratio becomes unity (the AC peak disappears), because the AC sweep rate becomes significantly faster than the reaction kinetics. The intermediate region, where the current ratio is strongly frequency dependent and exhibits a breakpoint frequency, is related to the standard charge transfer rate constant for the redox-active species. By fitting the experimental data (black squares in Figure 8) to the Randles model, we extract the rate constants for the monolayers comprised of P7 and P13, and for the Au electrodes, the recovered rate constants depend strongly on the length of the alkane chain anchoring the pyrene moiety to the electrode surface (k_{ct} = 1200 s^{-1} for P7 and 25 s^{-1} for P13).

It is instructive to consider qualitatively the differences in rate constant values for P7 and P13 in terms of through-bond tunneling that should depend exponentially on the distance and/or the number of C−C bonds in the anchoring chain. By assumption of typical bond lengths (1.79 Å for the C−S bond, 1.27 Å for each C−C bond, and 2.6 Å for the amide group),[28,31] we obtain the tunneling constant, β, from the experimental k_{ct} values

$$\ln(k_{ct}'/k_{ct}'') = \beta(d''-d') \quad (1)$$

where k_{ct}' and d' are rate constant and chain length of P7 and k_{ct}'' and d'' are the rate constant and chain length of P13. The use of a single tunneling constant, β, for different length anchoring chains warrants some explanation. The tether molecules, aside from their length, vary in the position of the amide group and the pyrene ring system relative to the substrate, but as was suggested in the literature, the contribution of an amide group to the electronic coupling is substantially similar to that of two methylene groups.[32,33] Because of the structural similarities of P7 and P13, we assumed the same tunneling constant for both molecules bound to the electrode surface. The structure-dependent tunneling constant is reflective of the decay of electronic coupling between the redox center and the electrode. Therefore, it should also reflect the nature of interactions between the tethered pyrene moieties and their immediate environment, which will include neighboring molecules within the monolayer and solvent molecules that have penetrated the interface. For P7 and P13 bound to gold, eq 1 yields a value of β = 0.44/Å, approximately half the literature value of 0.85/Å for a polymethylene chain.[34] A broad range of β values has been reported in the literature, ranging from the lowest values of 0.4−0.5 for conjugated bridges forming the tether molecules[28,35] and several proteins[36] to 0.8−1.0 for saturated alkanethiols and hydrocarbons.[30,35,37,38] However, it is important to note here that, for a monolayer such as P13 on gold, the chemical system is much more complex than the simple Randles approximation and it is not appropriate to fit the experimental data using a single rate constant (cf. Figure 8 right, R^2 = 0.95). In our opinion, our results suggest some disorder and dynamical

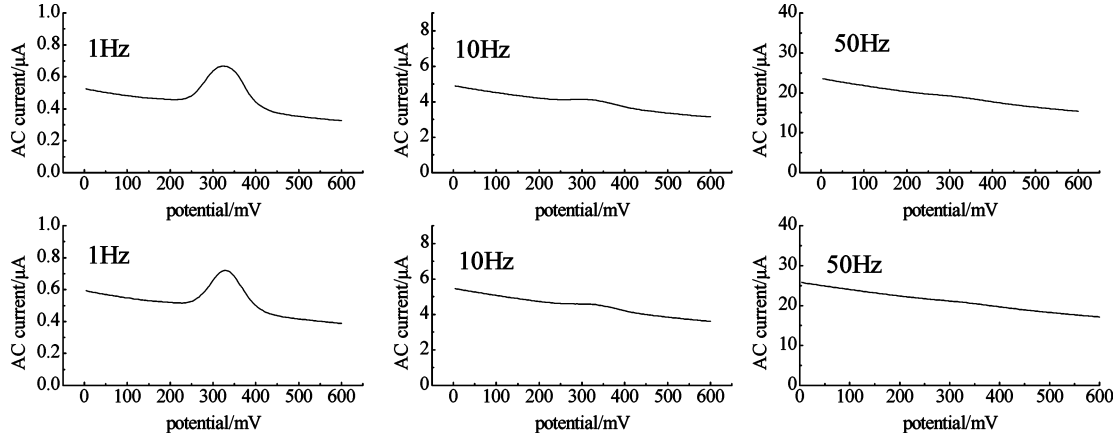

Figure 9. AC voltammograms for P8 (top row) and P19 (bottom row) on ITO in 1 M $HClO_4$.

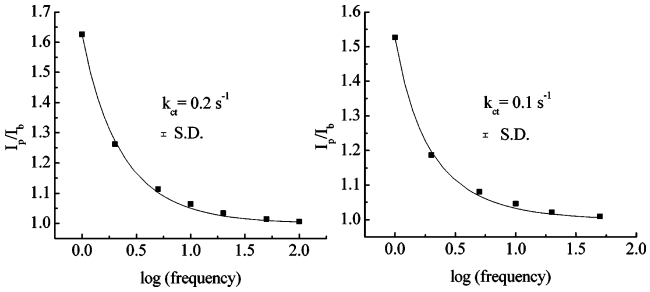

Figure 10. $I_{peak}/I_{background}$ vs log(frequency) plots of monolayers of P8 (left graph, $k_{ct} = 0.2\ s^{-1}$) and P19 (right graph, $k_{ct} = 0.1\ s^{-1}$) on ITO. The lines represent fits to the data (black squares) using a Randles equivalent circuit.

motions in these monolayers, leading to the presence of multiple populations of redox sites with a corresponding distribution of rate constants (and therefore the β values), likely due to a nonuniform orientational and spatial distribution of pyrene moieties within the monolayer. On that basis, the above discussion should be considered qualitative, with the central point being the structural complexity of the interface(s) we have reported here.

We have acquired the analogous AC voltammetry data and performed the same analysis for P8 and P19 on ITO. The data in Figure 9 show that the AC peak current diminishes more rapidly with increasing frequency and the fitting procedure yields much smaller k_{ct} values that are barely dependent on the anchoring chain length ($k_{ct} = 0.2\ s^{-1}$ for P8 and $0.1\ s^{-1}$ for P19, Figure 10). This result appears to be counterintuitive, in light of the data for gold substrates. We assume that the ester groups present on the tether chains reduce the rate of electron transfer in a manner analogous to that seen for ether groups,[39] making through-chain electron transfer inefficient. If this is in fact the case, the contribution of intermolecular interactions to the electron transfer process may become significant. Such a contribution could be the result of a highly disorganized interfacial structure, where the tethers of the pyrene derivatives as well as the pyrene rings form disorganized, aggregated structures, thereby maintaining the pyrene ring system at roughly the same average distance from the electrode surface for both P8 and P19.

As was the case for the data taken on a gold substrate, the AC peak position (in 1 M $HClO_4$) denotes the formal potential of these derivatives attached to ITO. We extract from the data a value of +328 mV, in very good agreement with the value of +324 mV obtained for a similar aminomethylpyrene derivative tethered to a gold substrate. This finding implies that the bond between the adlayer and the substrate plays a negligible role in the electrochemical responses of these interfaces. Apparently it is only the substituents in closest proximity to the ring system that can influence the redox properties of the pyrene moiety. The aliphatic chain, which mediates the spacing between the pyrene and the substrate, does not affect the redox properties of the ring system.

Pyrene Derivatives Nominally Buried within the Monolayer. The results we have considered to this point were obtained for pyrene derivatives, both on gold and ITO, which formed a sub-monolayer of molecules that face the aqueous solution. This system was characterized by substantial motional and structural freedom, as is seen in their electrochemical responses. We consider next our results for a family of interfaces where the pyrene ring system is buried within a mixed monolayer comprised of pyrene-containing species and aliphatic species. For all of the systems we consider, the mixed monolayers contained the same pyrene derivatives as were studied above, but they are coadsorbed with "diluent" molecules of longer hydrocarbon chains. For such systems we expect to observe changes in the electrochemical response of the pyrene moiety, related to the low dielectric environment provided by the diluent molecules, even though the cyclic voltammetry in the presence of the hydrophilic hexamine ruthenium(III) redox probe yielded quasireversible voltammograms (not shown), similar to those seen for the corresponding one-component monolayers. Octadecanethiol was the diluent for monolayers containing P7 and the hexadecylamide of mercaptoundecanoic acid was the diluent for monolayers containing P13 on gold substrates. Adipoylhexadecylamide was used as the diluent for monolayers containing P8, and the mono-(9-carboxy)-nonyl ester of adipic acid hexadecylamide was the diluent for monolayers containing P19 on ITO. Apparently, the coadsorbed diluent molecules do not improve the organization and passivation properties of the mixed monolayers compared to the one-component interfaces, and the electrochemical probe can diffuse to the electrode surface.

Figure 11 shows the CVs for P7 and P13 with coadsorbed diluents on gold and P8 and P19 with coadsorbed diluents on ITO. Two features of these voltammograms deserve closer inspection. The first is that the charge under the CV peaks is smaller than that for the corresponding one-component monolayers, a finding that we attribute to the coadsorption of two species that are competing for the same surface sites. For gold electrodes we recover a surface coverage of 3×10^{-11} mol/cm^2 for P7 diluted with octadecanethiol and 4×10^{-12} mol/cm^2 for P13 diluted with mercaptopropionic acid hexadecylamide. For the ITO substrates, we obtain a coverage of 8.4×10^{-12} mol/cm^2 for P8 diluted with adipoylhexadecylamide and

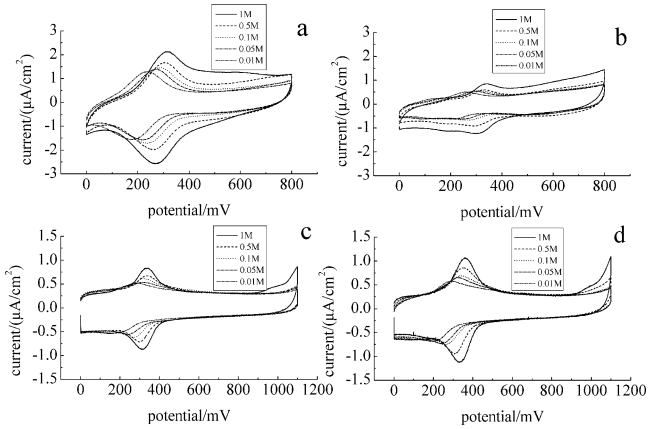

Figure 11. CVs for mixed monolayers: (a) P7 + diluent on gold; (b) P13 + diluent on gold; (c) P8 + diluent on ITO; (d) P19 + diluent on ITO in 1, 0.5, 0.1, 0.05, and 0.01 M aqueous $HClO_4$. The ionic strength for all measurements was maintained at 1 M by aqueous $LiCLO_4$. The sweep rate is 20 mV/s.

5.5×10^{-12} mol/cm^2 for P19 diluted with the mono-(9-carboxy)-nonyl ester of adipic acid hexadecylamide.

The other significant feature contained in these data is the splitting of the reduction peak and a "hump" on the oxidation wave of the CV curve for P13 confined within the two-component monolayer. As noted above, these two peaks can be assigned to 1,6-pyrenedione/1,6-dihydroxypyrene (a pair of CV peaks centered around 320 mV) and a contribution from the 1,8-pyrenedione/ 1,8-dihydroxypyrene redox couple at ca. 210 mV. This behavior is better resolved by AC voltammetry (Figure 12, bottom row, 1 Hz) and can be related to the coexistence of two derivatives in energetically well defined populations with relatively little interaction between the redox centers. These features were not seen for the corresponding one-component monolayers, suggesting that for the two-component monolayer the different pyrenequinone/diol isomers are stabilized by the presence of diluent molecules that separate the redox centers. For the two-component monolayer, the surface concentration of the pyrene derivative is almost 10 times smaller than that of the single-component monolayer, reducing the probability of interactions between different redox centers.

The results presented below are dominated by the 1,6-pyrenedione/1,6-dihydroxypyrene redox couple, which is seen as a pair of CV peaks centered around 320 mV. The 1,8-pyrenedione/1,8-dihydroxypyrene redox couple is seen only on gold for P13, with peaks centered around 130 mV. Figure 13 shows the midpoint potential, E_m, vs pH for the two-component monolayers on gold and ITO substrates. Similar to the data for the one-component monolayers, the slope of E_m vs pH is ca. −46 mV/pH unit for gold, regardless of the anchoring chain length, and ca. −49 mV/pH unit for ITO. We consider that these data also indicate a 1:1 proton-to-electron ratio to within the experimental uncertainty in the data, as discussed above for the

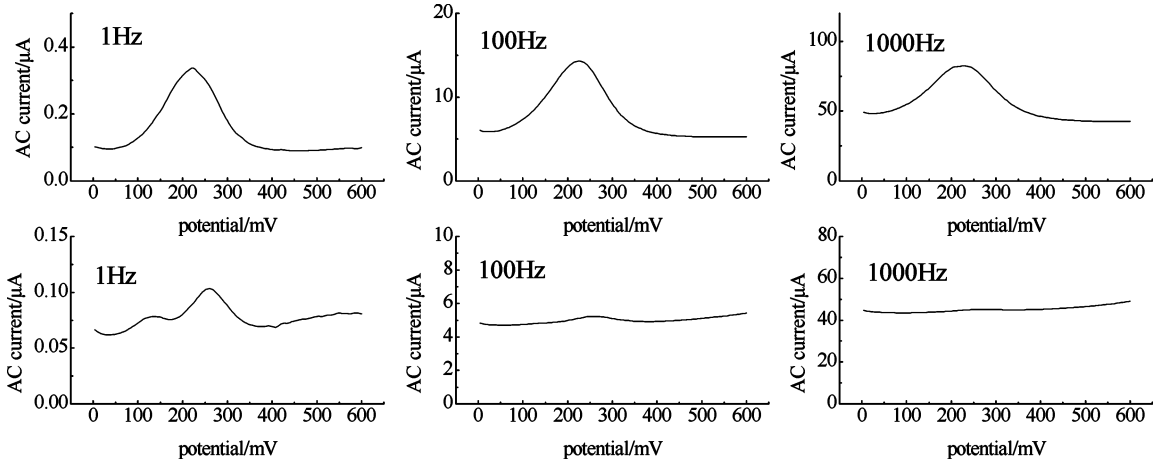

Figure 12. AC voltammograms for P7 + diluent (top row) and for P13 + diluent (bottom row) on gold in 0.1 M $HClO_4$.

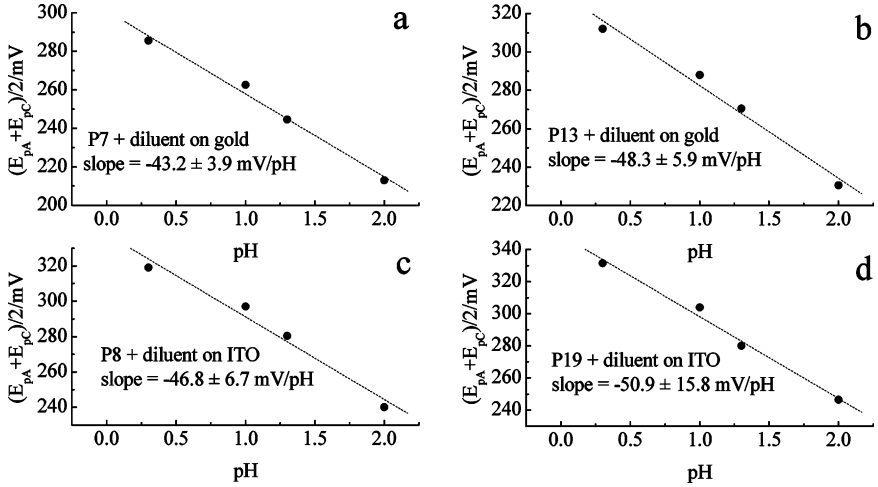

Figure 13. Dependence of the midpoint potential, E_m, on pH in 1 M $HClO_4$ aqueous solutions for (a) P7, slope = −43.2 ±3.9 mV/pH, and (b) P13, slope = −48.3 ± 5.9 mV/pH, in two-component monolayer structures, on gold and for (c) P8, slope = −46.8 ± 6.7 mV/pH, and (d) P19, slope = −50.9 ± 15.8 mV/pH, on ITO. The sweep rate is 20 mV/s for all scans. Uncertainties indicated in all panes are ±1σ.

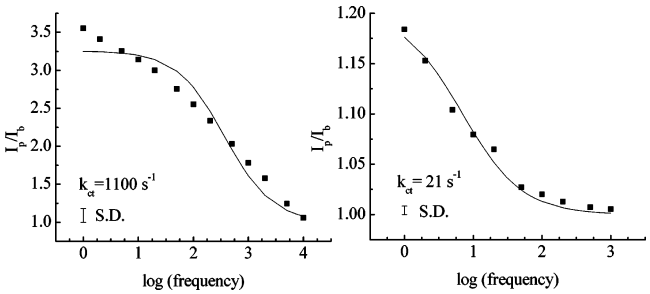

Figure 14. $I_{peak}/I_{background}$ vs log(frequency) plots of monolayers of P7 + diluent (left graph) and P13 + diluent (right graph) on gold. The solid lines represent fits to the data (black circles) using a Randles equivalent circuit.

case of single-component monolayers. These results show that, for our mixed two-component monolayers, the presence of diluent molecules has a negligible influence on the ratio of protons to electrons involved in the pyrene ring system redox reaction. The extrapolation of the slope in Figure 13 to pH = 0 gives the values of the formal potentials for the different pyrene derivatives in the mixed two-component monolayers. The values of +301 mV for the pyrenebutyric acid derivatives and +339 mV for the pyrenemethylamine derivatives are identical to those obtained for the corresponding one-component monolayers, underscoring the point that the presence of diluent molecules in the monolayer has no effect on the energetics of redox process. These two-component monolayers are not sufficiently compact to mediate the energetics of the pyrene redox chemistry.

To follow the kinetics of charge transfer in our mixed monolayer systems, we have performed AC voltammetry experiments analogous to those described above for one-component systems (Figure 12). The AC voltammograms for these two-component monolayers illustrate that, when the pyrene ring system is confined within a mixed monolayer interior, the AC current peak disappears at much lower frequencies than for the corresponding one-component monolayer. This finding suggests that the kinetics of charge transfer are slower for the two-component system, and we evaluate k_{ct} from plots of I_p/I_b vs log(frequency) (Figure 14). These fits yield $k_{ct} = 1100$ s^{-1} for P7 + diluent and 21 s^{-1} for P13 + diluent on gold. These findings show that the presence of diluent molecules slightly improves the spatial disorder of pyrene moieties within the monolayer.

The data in Figure 14 also show that P7 in a two-component monolayer yields a much more complex signal than the Randles approximation can account for, and the experimental data are not fit well using a single rate constant (Figure 14 left). Similar behavior has been reported for ferrocene confined within a two-component monolayer and such results have been explained in terms of multiple populations of redox sites, each with a different rate constant.[29,40] The data in Figure 14 point to the mixed monolayer structure containing multiple microenvironments for the pyrene rings, resulting in a distribution of electron-transfer rate constants. Our report of a single rate constant should thus be viewed as an average of the several rate constants that contribute to the experimental data.

Analogous experiments for the case of ITO electrodes covered with mixed adlayers containing P8 + diluent or P19 + diluent molecules (Figure 15, top and bottom rows, respectively) show that for these cases the charge-transfer kinetics of pyrene derivatives follow the same pattern as for P7 + diluent and P13 + diluent on gold. The presence of diluent molecules causes the AC voltammetry peak to disappear at lower frequencies as compared to a single-component layer with no diluent. Again, similar to the data for the gold surface, the pyrene ring system attached via a short tether (P8), seems to be less affected than P19 by the presence of diluent molecules. The AC voltammetry data obtained for a range of frequencies are fitted to the Randles model (Figure 16 left for P8 + diluent and Figure 16 right for P19 + diluent). It appears from these plots that, due to the available frequency range of the electrochemical instrumentation, we could get only a threshold of the I_p/I_b plot, as the charge-transfer kinetics on ITO are very slow. The resulting larger decrease in the charge-transfer rate constant for the case of P19 + diluent (from 0.1 s^{-1} without diluent to 0.008 s^{-1} with diluent), compared to the k_{ct} decrease for P8 (from 0.2 s^{-1} without diluent to 0.08 s^{-1} with diluent), is indicative of structural confinement and improved organization imposed on the electroactive chromophore by the presence of the diluent molecules. Relatively small differences in the rate constants, compared to the differences in chain lengths of the P8 and P19 molecules (18.8 Å for P8, 32.3 Å for P19), are not consistent with a tunneling mechanism for these data. An implication of these results, as for the single-component monolayers on ITO discussed above, is that these monomolecular layers are substantially disordered, with the pyrene moiety position within the layer not being dictated primarily by its tethering chain length. We note, however, that the presence of diluent molecules increases by a factor of 10 the difference in k_{ct} between the short (P8, $k_{ct} = 0.08$ s^{-1}) and long (P19, $k_{ct} = 0.008$ s^{-1}) molecules, in contrast to the data for the corresponding single-component layers (P8, $k_{ct} = 0.2$ s^{-1}; P19, $k_{ct} = 0.1$ s^{-1}).

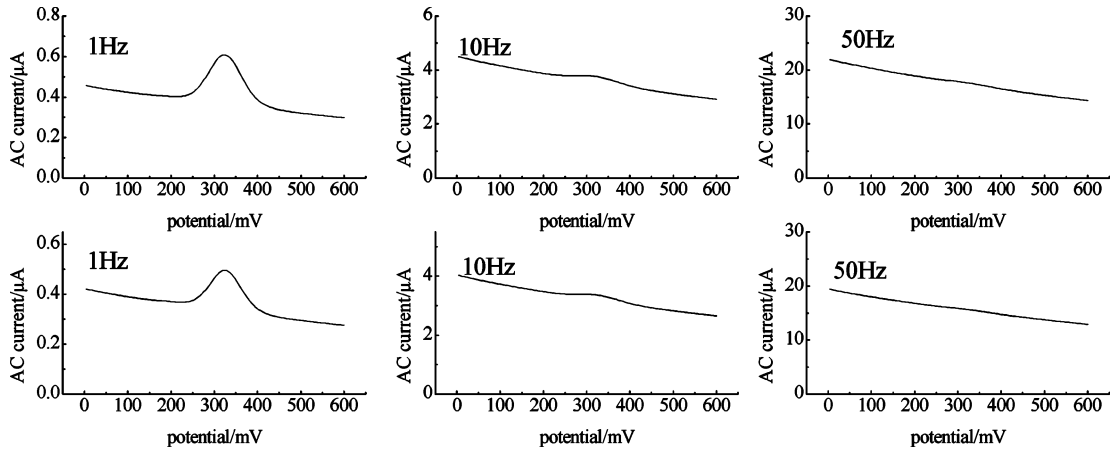

Figure 15. AC voltammograms for P8 (top row) and P19 (bottom row) on ITO in 1 M $HClO_4$.

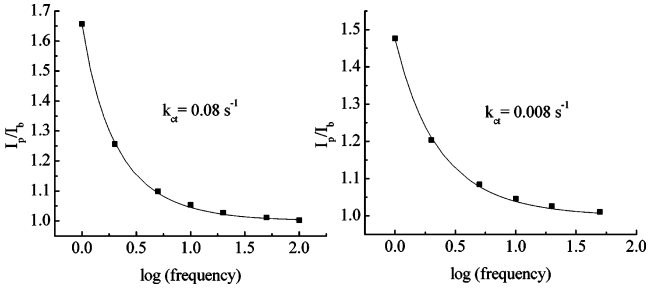

Figure 16. $I_{peak}/I_{background}$ vs log(frequency) plots of monolayers of P8 (left graph) and P19 (right graph) on ITO. The solid lines represent fits to the data (squares) using a Randles equivalent circuit. The size of symbol used for experimental data is larger than S.D..

Conclusions

We have synthesized and characterized a family of SAMs containing pyrene derivatives on gold and ITO substrates. When the covalently bound pyrene ring systems are the only constituents bound to the interfaces, their sub-monolayer coverage ranges from 4.4×10^{-11} mol/cm^2 for P7 and 1.7×10^{-11} mol/cm^2 for P13 on gold. Similar electrochemical evaluation for the modified ITO substrates yields values of 1.2×10^{-11} mol/cm^2 for P8 and 8.4×10^{-12} mol/cm^2 for P19. Electrochemical investigations show that these molecules do not form well-ordered, densely packed monolayers but enjoy significant structural freedom. The use of the Randles model for the evaluation of charge transfer kinetics, followed by the application of the tunneling model to qualitatively evaluate the film thickness dependence of the rate constant, reveal that the monolayers on gold are better organized than those formed on ITO. When the covalently bound pyrene ring systems are co-deposited at the interfaces with longer diluent molecules, the presence of these diluent molecules imposes some structural confinement on the tethered pyrene moieties and improved organization can be seen from the charge transfer kinetics, particularly on gold substrates. Yet these two-component monolayers are not sufficiently compact to mediate the energetics of pyrene redox chemistry. The issues of structural confinement, organization, and motional freedom within the monolayer are addressed in detail by means of steady-state and time-resolved emission spectroscopy in the accompanying article.

Acknowledgment. We are grateful to the U. S. Department of Energy for support of this work through Grant DEFG0299-ER15001 and to the Ministry of Scientific Research and Information Technology for support through Project No. PBZ 18-KBN-098/T09/2003 for the years 2004−2007.

References and Notes

(1) Nuzzo, R. G.; Allara, D. L. *J. Am. Chem. Soc.* **1983**, *105*, 4481.
(2) Allara, D. L.; Nuzzo, R. G. *Langmuir* **1985**, *1*, 45.
(3) Allara, D. L.; Nuzzo, R. G. *Langmuir* **1985**, *1*, 52.
(4) Karpovich, D. S.; Blanchard, G. J. *Langmuir* **1994**, *10*, 3315.
(5) Schessler, H. M.; Karpovich, D. S.; Blanchard, G. J. *J. Am. Chem. Soc.* **1996**, *118*, 9645.
(6) Lee, H.; Kepley, L. J.; Hong, H. G.; Akhter, S.; Mallouk, T. E. *J. Phys. Chem.* **1988**, *92*, 2597.
(7) Lee, H.; Kepley, L. J.; Hong, H. G.; Mallouk, T. E. *J. Am. Chem. Soc.* **1988**, *110*, 618.
(8) Burwell, D. A.; Thompson, M. E. *Chem. Mater.* **1991**, *3*, 730.
(9) Vermeulen, L. A.; Snover, J. L.; Sapochak, L. S.; Thompson, M. E. *J. Am. Chem. Soc.* **1993**, *115*, 11767.
(10) Putvinski, T. M.; Schilling, M. L.; Katz, H. E.; Chidsey, C. E. D.; Mujsce, A. M.; Emerson, A. B. *Langmuir* **1990**, *6*, 1567.
(11) Katz, H. E.; Schilling, M. L.; Chidsey, C. E. D.; Putvinski, T. M.; Hutton, R. S. *Chem. Mater.* **1991**, *3*, 699.
(12) Kohli, P.; Blanchard, G. J. *Langmuir* **2000**, *16*, 4655.
(13) Major, J. S.; Blanchard, G. J. *Chem. Mater.* **2002**, *14*, 2574.
(14) Krysinski, P.; Blanchard, G. J. *Bioelectrochemistry* **2005**, *66*.
(15) Gupta, P.; Ulman, A.; Fanfan, S.; Korniakov, A.; Loos, K. *J. Am. Chem. Soc.* **2005**, *127*, 4.
(16) Izdebski, J. *Preparatyka i elementy syntezy organicznej* **1983**, *17*, 836.
(17) Krysinski, P.; Brzostowska-Smolska, M. *J. Electroanal. Chem.* **1997**, *424*, 61.
(18) Mazur, M.; Blanchard, G. J. *J. Phys. Chem. B* **2004**, *108*, 1038.
(19) Moriconi, E. J.; Rakoczy, B.; O'Connor, W. F. *J. Org. Chem.* **1962**, *27*, 2772.
(20) Serfis, A. B.; Brancato S.; Fliesler, S. J. *BBA Biomembranes* **2001**, *1511*, 341.
(21) Kudelski A. *J. Raman Spectrosc.* **2003** *34*, 853.
(22) Wirde, M.; Gelius, U.; Nyholm, L. *Langmuir* **1999**, *15*, 6370.
(23) Michota, A.; Kudelski, A.; Bukowska, *J. Surf. Sci.* **2002**, *502*, 214.
(24) Gordillo, J. G.; Schiffrin, D. J. *Faraday Discuss.* **2000**, *116*, 89.
(25) Moncelli, M. R.; Herrero, R.; Becucci, L.; Guidelli, R. *Biochim. Biophys. Acta* **1998**, *1364*, 373.
(26) Moncelli, M. R.; Becucci, L.; Nelson, A.; Guidelli, R. *Biophys. J.* **1996**, *70*, 2716.
(27) Creager, S. E.; Wooster, T. T. *Anal. Chem.* **1998**, *70*, 4257.
(28) Creager, S.; Yu, C. J.; Bamdad, C.; O'Connor, S.; MacLean, T.; Lam, E.; Chong, Y.; Olsen, G. T.; Gozin, M.; Kayyem, J. F. *J. Am. Chem. Soc.* **1999**, *121*, 1059.
(29) Sumner, J. J., Creager, S. E. *J. Phys. Chem. B* **2001**, *105*, 8739.
(30) Sek, S.; Sepiol, A.; Tolak, A.; Misicka, A.; Bilewicz, R. *J. Phys. Chem. B* **2004**, *108*, 8102.
(31) Bain, C. D.; Troughton, E. B.; Tao, Y. T.; Whitesides, G. M.; Nuzzo, R. G. *J. Am. Chem. Soc.* **1989**, *111*, 321.
(32) Sumner, J. J.; Weber, K. S.; Hockett, L. A.; Creager, S. E. *J. Phys. Chem. B* **2000**, *104*, 7449.
(33) Sek, S.; Palys, B.; Bilewicz, R. *J. Phys. Chem. B* **2002**, *106*, 5907.
(34) Weber, K.; Hockett, L.; Creager, S. *J. Phys. Chem. B* **1997**, *101*, 8286.
(35) Sachs S. B.; Dudek S. P.; Hsung R. P.; Sita L.; Smalley J. F.; Newton, M. D.; Feldberg, S. W.; Chidsey, C. E. D. *J. Am. Chem. Soc.* **1997**, *119*, 10563.
(36) Kuki A. *Struct. Bonding* **1991**, *75*, 49.
(37) Slowinski, K.; Chamberlain, R. V.; Miller, C. J. K.; Majda, M. *J. Am. Chem. Soc.* **1997**, *119*, 11910.
(38) Kasmi, A. E.; Wallace, J. M.; Bowden, E. F.; Binet, S. M.; Linderman, R. J. *J. Am. Chem. Soc.* **1998**, *120*, 225.
(39) Napper, A. M.; Liu, H.; Waldeck, D. H. *J. Phys. Chem. B* **2001**, *105*, 7699.
(40) Li, J.; Schuler, K.; Creager, S. E. *J. Electrochem. Soc.* **2000**, 147 4584.